Hindawi
Advances in Materials Science and Engineering
Volume 2023, Article ID 6489920, 13 pages
https://doi.org/10.1155/2023/6489920

Research Article

Investigation of Magnesium and Chromium Fillers FSW Dissimilar Joint of AA6063 and AA 5154

Sangeetha Krishnamoorthi,[1] M. Prabhahar,[1] S. Prakash,[1] L. Prabhu,[1] K. Bhaskar,[2] Akhil V. Suku,[1] K. P. Shijindas,[1] S. L. Sooraj,[1] and A. Haiter Lenin[3]

[1]*Department of Mechanical Engineering, Aarupadai Veedu Institute of Technology, Vinayaka Mission's Research Foundation, Deemed to Be University, Salem, Tamil Nadu, India*
[2]*Department of Automobile Engineering, Rajalakshmi Engineering College, Rajalakshmi Nagar, Thandalam, Chennai 602 105, Tamil Nadu, India*
[3]*Department of Mechanical Engineering, Wollo University, Kombolcha Institute of Technology, Kombolcha, Ethiopia Post Box No: 208*

Correspondence should be addressed to A. Haiter Lenin; haiterlenina@gmail.com

Received 5 August 2022; Revised 20 October 2022; Accepted 24 November 2022; Published 24 January 2023

Academic Editor: J. T. Winowlin Jappes

Friction stir welding (FSW) is a solid-state metal joining process. There is no melting and recasting of metal while welding is used. Some of the defects commonly encountered in FSW are tunnel defect, bond, cracks, pin holes, and pipping defects. The defects occur because of improper metal mixing and less heat input in the weld nugget zone. In the fusion welding process, a filler rod is employed to form a quality weld with superior mechanical properties. In this work magnesium and chromium powders are used as filler materials. The purpose of this study is to ascertain whether filler materials and manufacturing processes have an impact on the weld nugget zone spot weld joint formation as well as the mechanical and abrasive properties of welded joints. This study's FSW filler materials mixing ratio and process parameters were improved by using the Central Composite Design (CCD) idea, which is discussed in more detail below Response Surface Methodology (RSM). The best empirical relationship between the parameters was provided by the CCD. The mathematical relationships were established to forecast the maximum tensile strength, maximum weld nugget hardness, and minimum corrosion rate by incorporating filler materials with process parameters. The optimal processing factors combination is predicted by conducting the validation test. The optimum parameters were the tool rotatory speed 600–1000 revolution per minute, welding speed 60 to 180 mm/min, plunge depth of 0.05 to 0.25 mm, center distance between the sample is 0–4 mm, as well as powder mixing ratio of 90 : 10, 92.5 : 7.5, 95 : 5, 97.5 : 2.5, and 100 : 0, the tensile test, microhardness, and corrosion rate analysis were conducted on the weld specimen. The welded test specimen provides better joint strength, weld nugget hardness, and enhanced corrosion resistance properties. The microstructure analysis shows the fine grain structure and homogeneous distribution of filler material with the base metal in the welded area.

1. Introduction

Welding is a critical step in the production process in which metals are fused together. Metal joining inventions have been bolstered by advances in metals and metal joining technology. Many industrial applications have seen a constant progress as a result of this. Bonding takes place at the original boundaries of the components during welding. It is heated to molten condition, and then allowed to cool down. There are two fundamental types of these processes: fusion welding and solid-state welding. Heat is utilised to melt the base metal during the fusion welding process. If you want a stronger joint, it is essential that the molten pool be enriched with additional filler metals. Arc welding, gas welding, resistance welding, laser beam welding, and electron beam welding are just a few of the common fusion welding methods. By applying pressure to the sites of contact, solid-state welding unites two metals at a temperature below their melting point.

The advancement of aluminum's pulsed GTAW technology and the primary properties of welds made of the AA 5154 alloy. The authors were identified that the use of current pulsing reduced the size of dendrite cells though improved mechanical properties were achieved [1]. Also, the use of helium gas as a shielding gas during pulsed GTAW of aluminium reduced the number of porosities, solidification cracking susceptibility, and weld distortion. In the postweld ageing of an AA6063 aluminium friction stir weld, the precipitation sequence is identified [2]. FSW has been shown to create a softened weld area. A minimum hardness zone is seen in the dissolved region. It has been discovered that hardness increases with postweld ageing. He conducted postweld ageing at 443 K.

After 12 hours, it was discovered that the welded area had a higher hardness level. The mechanical characteristics of Al-Si-Cu-Mg alloys were compared [3]. It was found that when the concentration of Cu and Mg is raised, the material's ductility decreases while its strength and ductility improve. The joint qualities of different cast A356 and wrought AA6063 were investigated by Cavaliere et al. [4], who changed the fixed location of the materials to alter the joint properties. For AA6063, the stir zone strength is larger than that of A356 when put on the retreating side during longitudinal tensile tests. When solution hardening, grain boundary migration happens because of an imbalance among thermodynamic driving forces and pinning forces, which causes grain expansion. Through solution heat treatment, the pinning forces are said to diminish as the solution temperature rises. The precipitate stages break down and the grains become coarser as the pinning forces decrease. As the temperature of the solution rises, so does the precipitate's dissolvability and coarsening.

AA 5154 aluminium alloy was utilised by Feng et al. [5] for FSW under various conditions, which include tool design and rotational and translational speed. According to microstructural, mechanical, and residual stress tests of four Al alloys AA 5154, thermal input rather than tool deformation affects welding parameters. To better understand the impacts of postweld heat treatment on 2219-O aluminium alloy microstructure and mechanical characteristics, Mindivan et al. [6] conducted a series of tests, tensile tests of heat-treated regions increase as solution temperature rises, up to 260% greater than the base metal's (BM) maximum allowable tensile strength.

Dissimilar friction stirs welded aluminium alloys enhanced with nano additions were studied [7]. Electrochemical methods were used to test the corrosion resistance of samples with and without nanoparticles. It is thought that the addition of MBT to CeMo containers during FSW increases the final material's corrosion resistance because it forms stable complexes with the alloying metals that prevent chloride from penetrating the AA surface.

Three different aluminum alloys, Al1050-H24, Al 6061-T6, and AlAA 5154-O, have the FSW. From the mechanical and metallurgical analysis, Al1050 consists of low deformation resistance and due to which the FSW joint made by a cylindrical pin tool exhibits high mechanical properties than the other types. But the shape of the tool pin does not affect the weldment microstructure and mechanical characteristics of 6061-T6 alloy weld joints [8, 9]. Deformation resistance in the FSW temperature range is relatively low for high melting temperature metals, hence cylindrical tools are better suited for these materials. But, also it is suitable for high deformation-resistant material with low rotational speed.

FSW properties and microstructural changes in aluminum alloy 6063-T6. A correlation between the tensile properties of the joints and a process parameter was examined according to their intended use and methodology. They used optical microscopy and microhardness measures to analyse the microstructures of several zones of FSW. Test welds mechanical resistance was observed to rise as welding speed was amplified at the same rotating speed [10]. They detected the source of tunnel (wormhole) faults in the weld nugget and the HAZ of an entity lower than that of fusion welds. In their tests, they used a variety of process parameters, but they could not regulate the downward force on the weld. Various parameter combinations were tested to see how far they could be taken. When welding speed is raised, the improvement in mechanical resistance provides an immediate economic benefit [11].

The characteristics of an FSW joint made of Al alloy with less porosity, fine microstructures, limited phase transition, and low oxidation to those of traditional welding techniques. They created FSWs of Al alloys AA 5154-H18 and 6111-T4 using certain FSW settings, and they measured the physical weld flaws [12]. Tensile tests and hardness dimensions were utilised to determine the microstructure of the weld and the BM, and these results were then correlated. They discovered that the AA 5154 specimens' stir zones are significantly softer than the strain-hardened foundation materials. Compared to the basic material, the SZs in 6111 are in terms of hardness. They discovered that some of the heat impacted zones of 6111 friction stir welding specimens exhibited natural ageing and hardening for up to 12 weeks following welding [13]. Welds made under specific welding conditions and in specific areas of the weld zone showed aberrant grain growth (AGG) after annealing AA 5154 FSW specimens. AGG is more severe in low-heat conditions, they discovered.

Aluminium alloy 6063-T6 friction stir welds were studied by their characteristics and microstructure. It was determined that the connection between tensile strength test results and a processing factor was high. Microstructures of several zones of FSW were shown and analysed using optical microscopy and microhardness extents [14, 15]. Test welds mechanical resistance was observed to rise as welding speed was increased at a constant rotational rate. Tunnel (worm hole) faults were discovered to be the result of a softening of the material in the weld nugget and the HAZ of an entity lower than that of fusion welding. In their tests, they used a variety of process parameters, but they could not regulate the downward force on the weld. They looked at the possibility of combining and extending the set of applicable parameters.

Friction stir welding of 6111 and AA 5154 aluminium alloys yielded minimal porosity, fine microstructures, and negligible phase transition as well as low levels of oxidation when the welding speed was increased [16]. They employed particular FSW parameters to build FSWs for aluminium

alloys AA 5154-H18 and 6111-T4 and then measured the physical weld flaws that resulted. The results of the tensile and hardness tests were related to the weld and base material microstructures. A significant difference was found between the AA 5154 specimens and the strain-hardened foundation materials in the softness of the stir zones. The SZs in the 6111 material have a hardness that is nearly identical to that of the base. According to their assessment of the heat-affected zone of 6111 friction stir welding specimens, this hardening remained for up to 12 weeks after the weld. Erroneous grain growth (EGG)was observed after annealing AA 5154 FSW specimens welded under particular circumstances. EGG is more severe in cooler climates, researchers found [17].

The fatigue fracture propagation behaviour of friction stir welded AA 5154-H32 and 6061-T651 aluminium alloys was investigated [18]. For dynamically recrystallized zone specimens, the stress intensity factor at residual stress (Kres) was used to calculate the residual stress-corrected K, or Kcorr, for FS welded plates that were subjected to residual stress measurements either perpendicular to or parallel to the welding direction. This was done to quantify the compressive residual stress' contribution to fatigue crack propagation rates. FS welded AA 5154-H32 and 6061-T651 specimens in the dynamically recrystallized zone showed fatigue crack propagation behaviour due to favourable compressive residual stress reduction effective K and detrimental grain refinement inducing intergranular fatigue failure, according to the authors.

The AA 5154 (Al-Mg) is mostly employed in marine environments, building construction, and food processing because of its corrosion resistance performed FSW on the AA 5154 aluminium alloy to discover the ideal process parameter to produce maximum corrosion resistance and mechanical qualities. It was decided to utilise the potentiodynamic polarisation test to see how well the material held up against corrosion [19]. The fine grain structure strengthens the anodic reactivity of the weld nugget. Optimal weld speed and feed resulted in the grain reinforcement and precipitate dissolution in the nugget zone which promotes passive film formation on the nugget portion during corrosion. Hence, high corrosion resistance was obtained.

Underwater FS welded Al AA 5154 alloy microstructure and mechanical behaviour were studied [20]. In this experiment, water-cooled specimens were found to have a much higher hardness of the stir zone than specimens cooled in air. Nan Zhou et al. (2018) studied the mechanical properties and fracture behaviour of AA 5154-H112 friction stir welds in relation to the kissing bond. An extensive welding matrix was used to weld the AA 5154-H112 at speeds ranging from 100 to 300 millimeters per second, with tool rotation rates between 800 and 1200 revolutions per minute. The duration of the kissing bond was influenced significantly by the welding parameters, particularly rotation and feed speeds, and the length of the kissing bond reduced as the welding heat input increased [21]. Tensile and fatigue fracture patterns were also discovered to be affected by kissing bond length and form. These cracks occurred in the welds with long fatigue life and strong tensile capabilities. Those with low fatigue life were found to have fractures in the kissing bond.

Several joint types can be fabricated by friction stir welding (FSW), namely butt-, lap- (overlap-), and T-lap joints (Figure 1) along with the lap joint in the form of spot welding by friction stir spot welding (FSSW).

Then, to enhance the FSW variables, multiobjective optimization techniques including central composite design and response Surface optimization were applied. This friction stir weld connection of aluminium alloy 6063 and aluminium alloy AA 5154 has been studied only in the context of metallurgical, mechanical, and corrosion behaviour. But, no visible investigation has been completed on FSW connections with filler metal addition to dissimilar material joining of AA6063 and AA 5154 aluminium.

Hence, it is more interesting to investigate the effect of addition of filler to dissimilar material joining of AA6063 and AA 5154 aluminium alloy with regard to its metallurgical, mechanical, and corrosion behaviours. The focus of the current study is therefore on the connection of aluminium alloys such as AA6063 and AA 5154 that have different compositions, as well as the inclusion of filler material. Mg increase in the weld zone improved the weld connections TS.

2. Materials and Methodology

The Al alloy 6063 and AA 5154 were selected as base materials. The fillers magnesium and chromium were selected to introduce between the joints during the welding in powder form. The fillers were stuffed into the holes on butting of the plate to be welded. The tungsten carbide was selected as a tool material. The hexagonal pin profile was preferred for this work due to its good stirring characteristics. The optimum parameters were the tool rotatory speed 1000 revolution per minute, welding speed 120 mm/min, plunge depth of 0.15 mm, mid distance among the holes of 2 mm, as well as powder mixing ratio of 95 : 5 (%). The tensile test, microhardness, and micro- and macrostructure analyses were conducted on the weld specimen.

2.1. Evaluation of Base Metal Composition and Properties. Aluminium alloys AA6063 and AA 5154 were employed as the base metals in this study. The chemical composition of base metals was attained from vacuum spectrometer (ARL-Model3460). A spectroscopic analysis was performed to determine the alloying elements by igniting sparks at various locations on the base metal samples. Table 1 shows the percentage of chemical characteristics of each element in AA515 and AA6063. The physical and mechanical characteristics of AA 5154 and AA6063 are shown in Table 2.

ASTM E8M-04 criteria were used to prepare tensile test samples for base metals. Figure 2 depicts the base metals' microstructure. Strengthening precipitates are distributed uniformly across the microstructure, which primarily comprises of elongated grains.

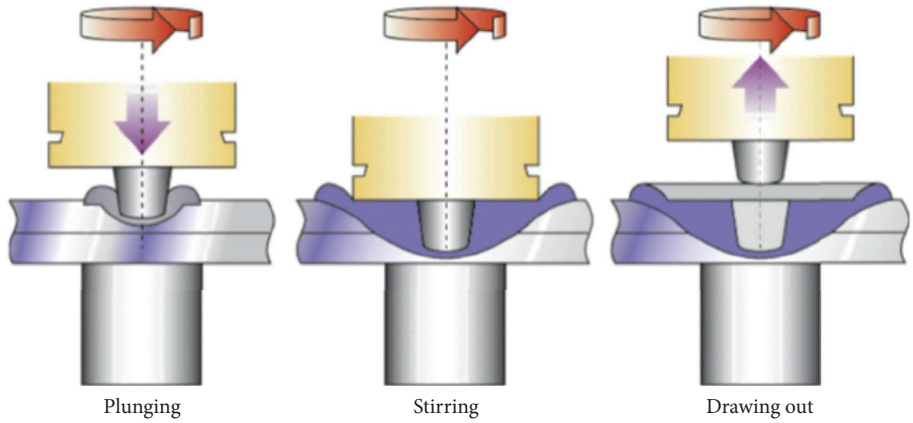

Figure 1: Schematic illustration of friction stir spot welding.

Table 1: Chemical properties of AA 5154 and AA6063.

Fundamentals	Wt % of AA 5154	Wt % of AA6063
Magnesium	2.8	0.82
Silicon	0.25	1.0
Chromium	0.35	0.05
Manganese	0.10	0.52
Ferrous	0.40	0.27
Copper	0.10	0.02
Zinc	0.10	0.1
Titanium	0.05	0.03
Aluminium	Remaining	Remaining

Table 2: Physical and mechanical characteristics of AA 5154 and AA6063.

Fundamentals	Units	AA 5154	AA6063
Density	(g/cm^3)	2.68	2.700
Vickers hardness	(HV)	85	120
Melting point	(°C)	607	555
Elongation	(%)	27	13
Ultimate tensile strength	(MPa)	217	330
Yield strength	(MPa)	193	279

2.2. Levels of Process Parameters. The settings for the test runs were derived from references to the literature for AA 5154, AA6063, and a different combination of the two alloys. Trials were completed in order to stabilize procedure parameter and eliminate any visible faults in the joints. Based on these tests, the freezing process parameters were as follows: tool rotating speed of 1000 rpm, welding speed of 120 milli meter/s, and a plunge depth of 0.15 millimeter. The frozen parameter was confirmed by welding three samples together. The strength of the welded junction was put to the test. A total of 147 MPa tensile strength was achieved by this combination. Table 3 shows the tensile strength for the freezing parameters as determined by the trial experiments.

There were a number of variables that were taken into consideration during the experiment. Welding speeds ranged since 600 rpm up to 1400 rpm as well as 60 millimeter/min up to 180 milli meter/min after a series of testing. From 0.05 mm to 0.25 mm, the depth of the plunge was steadily raised in five 0.05 mm steps. It was decided that the center distance would be spaced at intervals ranging from 0 millimeters to 4 millimeters apart along the plate's butting surface, 2 millimeters and 3 millimeters. In the welding stir zone, the mean wt. percentages of chromium and magnesium are measured. The average wt. percentage of Mg and Cr alloy elements in the weld stir zone was utilised to calculate wt. % proportion. The entire filler wt. was used to compute the Mg/Cr filler % proportion. A 90 : 10, 92.5 : 7.5, 95 : 5, 97.5 : 2.5, and 100 : 0 mixture of Mg and Cr powders was employed. The hexagonal pin profile has a 20 mm shoulder diameter, an 8 mm pin diameter, and an overall 7.6 mm length. Table 4 shows the FSW process parameters, as well as their range and level.

3. Results and Discussion

3.1. Tensile Strength. This test was carried out on 32 FSW samples, and the results are tabulated in Table 5 below.

3.2. ANOVA for Tensile Strength. ANOVA was utilised to assess in developing an actual connection. The ANOVA tests for TS are displayed in the image and are included in Table 6. We can conclude that the model's F-value of 382.31 is statistically significant. It is impossible for noise to produce an F-value this enormous with a 0.01 percent chance. Modelling terms are considered significant when their p values fall below 0.05. It is important to note that R2, W2, P2, C2, and M2 are all relations of reference in this example.

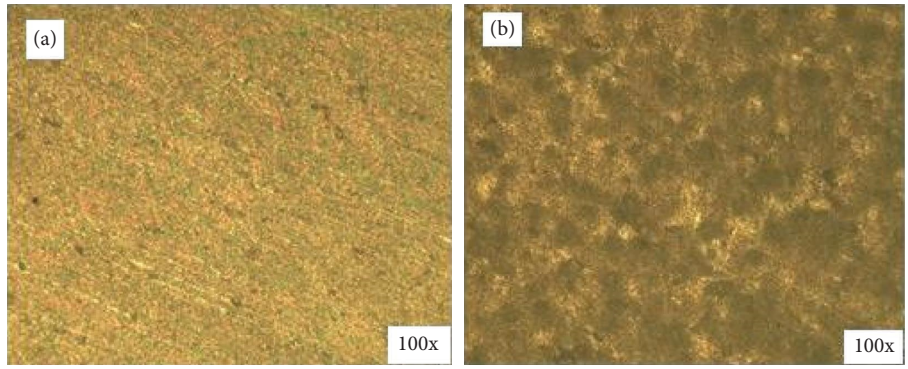

Figure 2: Optical micrograph of base metals (a) AA 5154 and (b) AA6063.

Table 3: FSW process parameters.

Parameter	Tensile strength (MPa)		
Tool rotating speed 1000 rpm, welding speed 120 mm/min, and plunge depth 0.15 mm	Experiment 1	Sample 1	145
		Sample 2	148
		Sample 3	147
	Experiment 2	Sample 1	146
		Sample 2	149
		Sample 3	145
	Experiment 3	Sample 1	147
		Sample 2	146
		Sample 3	148
Average tensile strength			147

Table 4: Processing factors with their range and levels.

S. no.	Factors	Factor levels				
		(−2)	(−1)	(0)	(1)	(2)
1	R-tool rotational speed (rpm)	600	800	1000	1200	1400
2	W-welding speed (mm/min)	60	90	120	150	180
3	P-plunge depth (mm)	0.05	0.10	0.15	0.20	0.25
4	C-center distance (mm)	0	1	2	3	4
5	M-powder mixing ratio (Mg : Cr) (%)	90 : 10	92.5 : 7.5	95 : 5	97.5 : 2.5	100 : 0

Statistically significant model terms are those with a value greater than 0.1. Weld joint tensile strength is evaluated using the following empirical relationships:

$$\begin{aligned} TS = \{&172.47 + 2.62(R) + 2.21(W) + 1.12(P) + 0.9583(C) \\ &+ 0.7917(M) + 0.6875(RM) + 0.9375()\text{–}9.375(\text{WC}) \\ &\text{–}0.5625(\text{WM})\text{–}1.44(\text{PC}) + 0.6875(\text{PM}) \\ &+ 0.5625(CM)\text{–}5.72\left(\text{R}^2\right)\text{–}6.34\left(\text{W}^2\right)\text{–}6.72\left(\text{P}^2\right) \\ &\text{–}5.59\left(\text{C}^2\right)\text{–}6.22\left(\text{M}^2\right)\}\text{MPa}. \end{aligned} \quad (1)$$

As can be seen from the F-statistic, a failure to fit is not substantial when compared to the total error. Noise has a 13.69 percent probability of causing such a significant inadequacy in the F-value. Less than 0.2 of a difference exists between the expected R2 of 0.9699 and the adjusted R2 of 0.9960. The SN ratio is determined by adequate precision. There should be a ratio of at least 4 is to 1. In this model, a signal strength of 63.916 is considered acceptable. The design space can be guided by this paradigm. Figure 3 shows the FRW process. Figure 4 depicts the tensile sample prior to and following its testing procedure.

3.3. Microhardness. Thirty-two FSW samples were tested for microhardness, and the findings are shown in Table 7. AA6063 and AA 5154 dissimilar alloys are presented for the influence of process factors on the microhardness of each alloy.

Figure 5 shows the weld cross section of the AA 5154-AA6063 dissimilar joint at the AS and RS side showing that the FSZ, the weld's butting surface was tested for microhardness. As opposed to the moving side, the friction stir zone (FSZ) weld

Table 5: Design matrix for tensile strength.

Trial no.	Experiment particulars					Results
	Input factors					Responses
	R	W	P	C	M	TS (MPa)
1	800	90	0.05	1	97.5 : 2.5	132
2	1200	150	0.2	2	97.5 : 2.5	145
3	600	120	0.1	1	92.5 : 7.5	140
4	1200	90	0.2	3	92.5 : 7.5	140
5	800	180	0.1	1	92.5 : 7.5	139
6	1000	90	0.2	2	97.5 : 2.5	144
7	800	150	0.25	1	97.5 : 2.5	145
8	1200	90	0.2	3	92.5 : 7.5	140
9	600	150	0.1	3	92.5 : 7.5	146
10	1200	90	0.1	3	97.5 : 2.5	148
11	1000	180	0.1	3	97.5 : 2.5	140
12	1200	150	0.1	4	92.5 : 7.5	146
13	800	90	0.2	3	97.5 : 2.5	139
14	1200	120	0.2	3	92.5 : 7.5	140
15	800	150	0.2	4	92.5 : 7.5	142
16	1200	150	0.2	3	97.5 : 2.5	149
17	600	120	0.15	2	95.0 : 5.0	145
18	1400	120	0.25	2	95.0 : 5.0	154
19	1000	60	0.15	2	95.0 : 5.0	143
20	1000	180	0.15	2	95.0 : 5.0	151
21	1000	120	0.05	2	95.0 : 5.0	143
22	1000	120	0.25	2	95.0 : 5.0	148
23	1000	120	0.05	0	95.0 : 5.0	148
24	1000	120	0.15	4	95.0 : 5.0	152
25	1000	120	0.05	2	90.0 : 10.0	145
26	1000	120	0.15	4	100.0 : 0.0	150
27	1000	120	0.05	2	95.0 : 5.0	172
28	1000	120	0.15	2	95.0 : 5.0	173
29	1000	120	0.05	4	95.0 : 5.0	172
30	1000	120	0.15	2	95.0 : 5.0	173
31	1000	120	0.25	4	95.0 : 5.0	172
32	1000	120	0.15	2	95.0 : 5.0	173

hardness was discovered to be higher, as associated to both advancing and retreating sides. The stir zone weld's hardness is determined by the welding process' parameters. The weld's microhardness was raised, thanks to the stir zone's grain refining and grain particle size reduction. The manufactured junction with a rotating speed of 600 rpm had the lowest weld hardness measured. As shown in Figure 5, the friction stir zone had the highest microhardness value of 93 HV at the AS side and fine grain structure with 34 HV at the RS side, when the tool was rotated at 1000 rpm. With these parameters are in place, we achieved the highest weld hardness in comparison to any other process parameter levels: welding speed of 120 m/s, plunge depth of 0.15 mm, center distance along 2 mm as well as a 95 percent Mg, 5 percent Cr, powder mix proportion (Figure 6(a)), R-tool rotational speed (rpm) (Figure 6(b)), W-welding speed (mm/min) (Figure 6(c)), P-plunge depth (mm) (Figure 6(d)), C-center distance (mm) (Figure 6(e)), and M-powder mixing ratio (Mg : Cr) (%).

3.4. ANOVA for Microhardness. Table 8 displays the results of an ANOVA test to determine the microhardness of a sample. The model's F-value of 84.15 indicates its significance. A noise-induced F-value this big has a vanishingly small probability of occurrence. Model terms that have a p value below 0.05 are considered significant. Equation (2) represents the final empirical relationship to estimate the microhardness of the weld area.

$$\begin{aligned} MH = \Big\{ & 91.95 + 6.14(R) + 1.55(W) + 1.55(P) + 2.14(C) \\ & + 1.22(M) + 0.9376(RP) - 1.32() - 0.9376(\mathrm{WC}) \\ & - 0.8126(\mathrm{WM}) - 0.9376(\mathrm{PC}) - 0.8126(\mathrm{PM}) \\ & - 0.6876(\mathrm{CM}) - 3.83\left(\mathrm{R}^2\right) - 3.45\left(\mathrm{W}^2\right) - 3.19\left(\mathrm{P}^2\right) \\ & - 2.19\left(\mathrm{C}^2\right) - 2.69\left(\mathrm{M}^2\right) \Big\} \mathrm{HV}. \end{aligned} \tag{2}$$

F-value of 0.767 indicates that the lack of fit is statistically insignificant when compared to the pure error. Noise has a 62.67% risk of causing a substantial lack of fit F-value. The predicted R2 of 0.9124 is regarded fair because the difference between the predicted R2 and the adjusted R2 is lesser than 0.2. The signal-to-noise ratio was assessed using adequate precision. There should be a ratio of at least 4 is to 1.28.7479 as a suitable signal in this model.

Table 6: Tensile strength ANOVA results.

Sources	SS	Dof	Mean square	F-value	P value	Significance
Model	4582.41	20	4582.41	383.32	<0.0001	Significant
R*	164.38	1	164.38	277.02	<0.0001	
W*	118.05	1	118.05	196.34	<0.0001	
P*	31.38	1	31.38	50.79	<0.0001	
C*	23.05	1	23.05	37.89	<0.0001	
M*	16.05	1	16.05	26.2	0.0005	
RW	1.55	1	1.55	3.62	0.1347	
RP	1.55	1	1.55	3.62	0.1347	
RC	0.0632	1	0.0632	0.1053	0.7529	
RM*	7.57	1	7.57	13.63	0.0046	
WP*	13.07	1	13.07	24.48	0.0006	
WC*	14.07	1	14.07	24.48	0.0006	
WM*	5.07	1	5.07	8946	0.0144	
PC*	32.07	1	32.07	56.28	<0.0001	
PM*	7.61	1	7.61	13.63	0.0046	
CM*	5.06	1	5.06	9.46	0.0144	
R^{2*}	957.47	1	958.47	1589.49	<0.0001	
W^{2*}	1181.31	1	1181.31	1978.39	<0.0001	
P^{2*}	1323.03	1	1323.03	2208.1	<0.0001	
C^{2*}	916.91	1	916.91	1531.29	<0.0001	
M^{2*}	1133.37	1	1133.37	1892.55	<0.0001	
Residual	6.69	11	0.5992			
Lack of fit	5.08	6	0.8485	2.84	0.1369	Not significant
Pure error	1.4	5	0.3			
Cor total	4586.86	31				
Std. deviation	0.7743		R^2	0.9987		
Mean	148.54		AdjustedR^2	0.9960		
CV (%)	0.5178		Predicted R^2	0.9698		
PRESS	139.08		Adeq. precision	63.9173		

*Significant factor.

Figure 3: Friction stir welding.

Thirty-two FSW samples were tested for corrosion rate, and the findings are shown in Table 9. AA6063 and AA 5154 dissimilar alloys are presented for the influence of process factors on the corrosion rate of each alloy.

3.5. ANOVA for Corrosion Rate. The analysis of variance test results for the rate of deterioration are tabulated in Table 10. Noise has a 0.01 percentage probability of producing an F-value of this size. P values of lesser than 0.05 are considered significant in the model's terms. As shown in equation (3), the empirical relationships used to determine the weld surface corrosion rate are represented as follows.

$$\begin{aligned} CR = \{&1.13 + 0.3166\,(R) - 0.294\,(\mathrm{W}) - 0.147\,(\mathrm{P}) + 0.1809\,(\mathrm{C}) \\ &+ 0.26\,(M) + 0.2036\,(RW) + 0.3054\,(RP) \\ &- 0.2206\,(\mathrm{RM}) - 0.1526\,(\mathrm{WM}) - 0.2206\,(\mathrm{PC}) \\ &- 0.1696\,(\mathrm{CM}) + 0.8868\,(\mathrm{R2}) + 0.8868\,(\mathrm{W2}) \\ &+ 0.361\,(P2) + 0.5306\,(C2) + 0.6833\,(M2)\}\,\frac{mm}{y}. \end{aligned} \tag{3}$$

Negative values indicate that the terms of reference are insignificant. According to the F-value of 1.04, the lack of fitting is insignificant when compared to the total

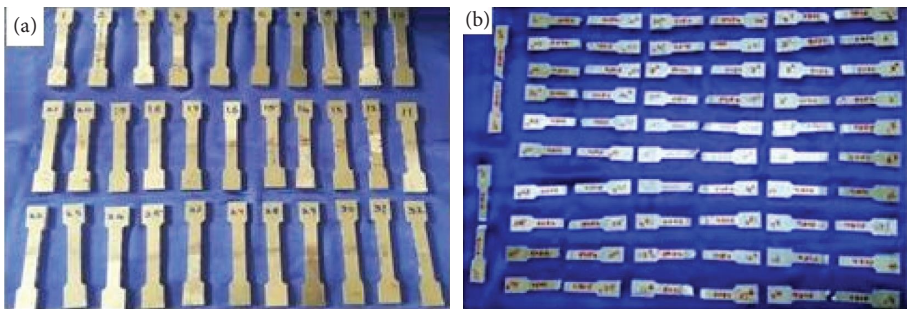

Figure 4: Tensile sample before and after testing.

Table 7: Design matrix for microhardness.

Trial no.	Experimental details: Input factors R (rpm)	W (mm/min)	*P* (mm)	C (mm)	M (%)	Results: Responses MH (HV)
1	600	120	P	C	97.5 : 2.5	68
2	1200	150	0.05	1	97.5 : 2.5	70
3	800	90	0.2	2	92.5 : 7.5	67
4	1200	150	0.1	1	97.5 : 2.5	85
5	1000	180	0.2	3	92.5 : 7.5	68
6	1200	90	0.1	1	97.5 : 2.5	86
7	800	150	0.2	2	97.5 : 2.5	72
8	1200	150	0.25	1	92.5 : 7.5	86
9	1000	120	0.2	3	92.5 : 7.5	71
10	1200	90	0.1	3	97.5 : 2.5	85
11	1000	180	0.1	3	97.5 : 2.5	76
12	1200	150	0.1	3	92.5 : 7.5	86
13	800	90	0.1	4	97.5 : 2.5	75
14	1200	90	0.2	3	92.5 : 7.5	88
15	1000	180	0.2	3	92.5 : 7.5	74
16	1200	150	0.2	4	97.5 : 2.5	87
17	600	120	0.2	3	95.0 : 5.0	66
18	1400	150	0.15	2	92.5 : 7.5	87
19	1000	60	0.25	2	95.0 : 5.0	74
20	1000	150	0.15	2	92.5 : 7.5	86
21	1000	120	0.15	2	95.0 : 5.0	77
22	1000	120	0.05	2	95.0 : 5.0	82
23	1000	120	0.25	2	95.0 : 5.0	80
24	1000	120	0.05	0	95.0 : 5.0	86
25	1000	120	0.15	4	90.0 : 10.0	79
26	1000	120	0.05	2	100.0 : 0.0	83
27	1000	120	0.15	4	95.0 : 5.0	93
28	1000	120	0.05	2	95.0 : 5.0	93
29	1000	120	0.15	2	95.0 : 5.0	92
30	1000	120	0.05	4	95.0 : 5.0	91
31	1000	120	0.15	2	95.0 : 5.0	93
32	1000	120	0.25	4	95.0 : 5.0	90

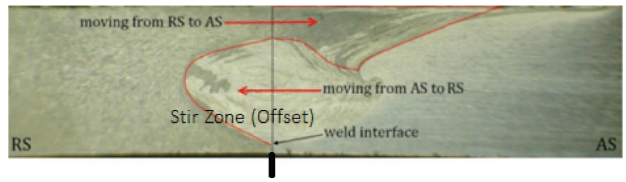

AS-Advancing Side
RS-Retreating Side
FSZ-Friction Stir Zone

Figure 5: Weld cross section of the AA 5154-AA6063 dissimilar joint at the AS and RS side showing the FSZ.

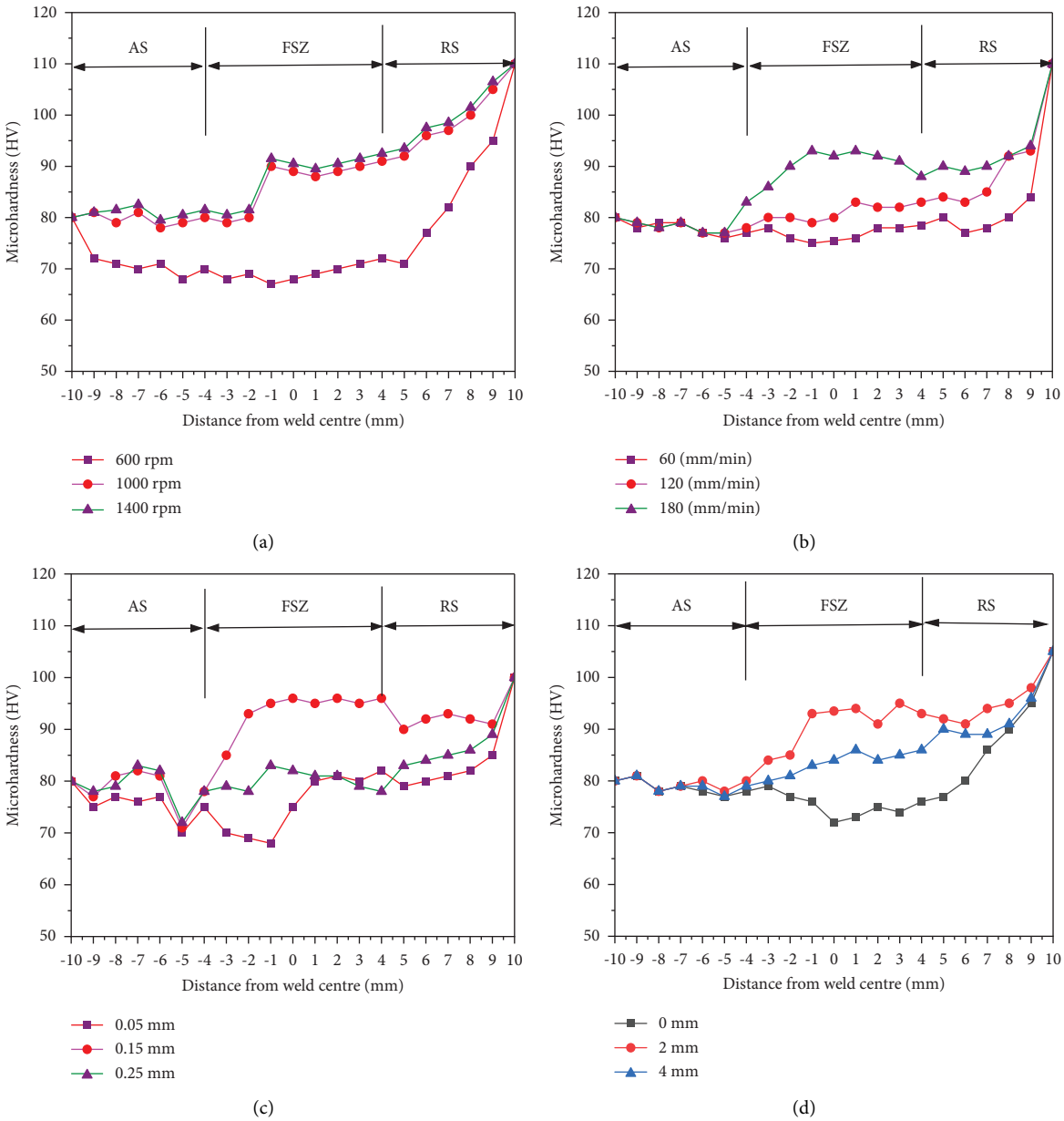

Figure 6: Continued.

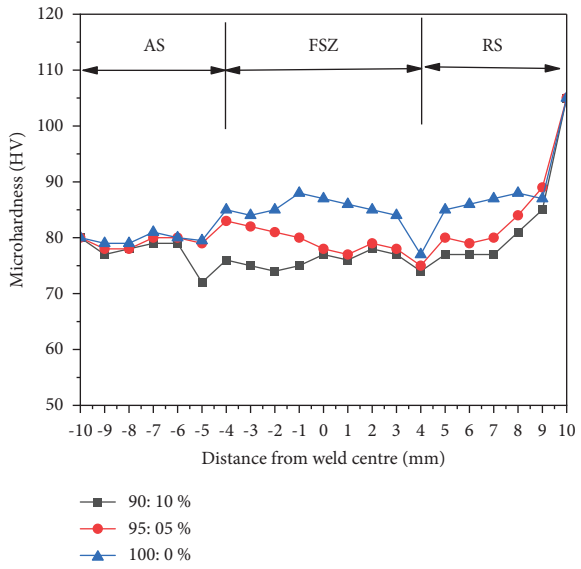

(e)

Figure 6: Impact of processing factors on microhardness of AA6063 and AA 5154 (a) R, (b) W, (c) P, (d) C, and (e) M.

Table 8: Microhardness ANOVA results.

Sources	SS	Dof	Mean square	*F* value	*P* value	Significance
Model	2360.52	20	2360.52	85.16	<0.0001	Significant
R*	901.48	1	901.48	645.75	<0.0001	
W*	58.05	1	58.05	41.85	<0.0001	
P*	58.05	1	58.05	41.85	<0.0001	
C*	107.41	1	107.41	78.58	<0.0001	
M*	36.05	1	36.05	26.08	0.0005	
RW	3.07	1	3.07	2.18	0.1672	
RP*	15.08	1	15.08	10.08	0.0091	
RC	0.4625	1	0.4625	0.4031	0.5388	
RM	4.07	1	4.07	2.18	0.1668	
WP*	28.55	1	28.55	20.74	0.001	
WC*	15.05	1	15.05	10.08	0.0099	
WM*	10.57	1	10.57	8.57	0.0191	
PC*	15.05	1	15.05	10.08	0.0088	
PM*	10.57	1	10.57	8.57	0.0188	
CM*	8.55	1	8.55	5.42	0.0402	
R^{2} *	427.64	1	427.64	306.19	<0.0001	
W^{2}*	347.76	1	347.76	248.98	<0.0001	
P^{2}*	299.09	1	299.09	214.14	<0.0001	
C^{2}*	241.09	1	241.09	101.02	<0.0001	
M^{2}*	212.76	1	212.76	152.33	<0.0001	
Residual	1638	12	1.5			
Lack of fit	8.335	7	1.24	0.758	0.6268	Not significant
Pure error	9	6	1.7			
Cor total	2465.89	32				
Std. deviation	1.19		R^{2}	0.9935		
Mean	80.44		Adjusted R^{2}	0.9817		
CV (%)	1.47		Predicted R^{2}	0.9124		
PRESS	207.14		Adeq. precision	28.7479		

Table 9: Design matrix for corrosion rate.

Trial no.	Experimental particulars / Input factors R (rpm)	W (mm/min)	P (mm)	C (mm)	M (%)	Results / Responses CR (mm/y)
1	800	90	**P**	**C**	97.5 : 2.5	5.427
2	1200	90	0.05	1	92.5 : 7.5	4.206
3	800	150	0.2	2	92.5 : 7.5	3.256
4	1200	150	0.1	1	97.5 : 2.5	3.934
5	800	90	0.2	3	92.5 : 7.5	3.256
6	1200	90	0.1	1	97.5 : 2.5	5.427
7	800	150	0.2	2	97.5 : 2.5	3.799
8	1200	150	0.25	1	92.5 : 7.5	4.749
9	800	90	0.2	3	92.5 : 7.5	5.156
10	1200	90	0.1	3	97.5 : 2.5	4.884
11	800	150	0.1	3	97.5 : 2.5	4.613
12	1200	150	0.1	3	92.5 : 7.5	5.427
13	800	90	0.1	4	97.5 : 2.5	4.477
14	1200	90	0.2	3	92.5 : 7.5	4.613
15	800	150	0.2	3	92.5 : 7.5	3.12
16	1200	150	0.2	4	97.5 : 2.5	4.749
17	600	120	0.2	3	95.0 : 5.0	4.07
18	1400	120	0.15	2	95.0 : 5.0	5.427
19	1000	60	0.25	2	95.0 : 5.0	5.563
20	1000	180	0.15	2	95.0 : 5.0	3.934
21	1000	120	0.15	2	95.0 : 5.0	2.849
22	1000	120	0.05	2	95.0 : 5.0	2.442
23	1000	120	0.25	2	95.0 : 5.0	2.985
24	1000	120	0.05	0	95.0 : 5.0	3.663
25	1000	120	0.15	4	90.0 : 10.0	3.256
26	1000	120	0.05	2	100.0 : 0.0	4.613
27	1000	120	0.15	4	95.0 : 5.0	1.486
28	1000	120	0.05	2	95.0 : 5.0	1.085
29	1000	120	0.15	2	95.0 : 5.0	0.814
30	1000	120	0.05	4	95.0 : 5.0	1.221
31	1000	120	0.15	2	95.0 : 5.0	0.949
32	1000	120	0.25	4	95.0 : 5.0	1.085

Table 10: ANOVA test results for corrosion rate.

Sources	Sum of squares	Degree of freedom	Mean square	F-value	*P* value	Significance
Model	68.4	20	3.42	62.3	<0.0001	Significant
R*	2.41	1	2.41	43.84	<0.0001	
W*	2.08	1	2.08	37.8	<0.0001	
P*	0.5183	1	0.5183	9.44	0.0106	
C*	0.7852	1	0.7852	14.3	0.003	
M*	1.62	1	1.62	29.57	0.0002	
RW*	0.663	1	0.663	12.08	0.0052	
RP*	1.49	1	1.49	27.19	0.0003	
RC	0.0046	1	0.0046	0.0836	0.7778	
RM*	0.7784	1	0.7784	14.18	0.0031	
WP	0.0738	1	0.0738	1.35	0.2706	
WC	0.1151	1	0.1151	2.1	0.1755	
WM*	0.3724	1	0.3724	6.78	0.0245	
PC*	0.7784	1	0.7784	14.18	0.0031	
PM	0.2259	1	0.2259	4.11	0.0674	
CM*	0.46	1	0.46	8.38	0.0146	
R^{2*}	23.07	1	23.07	420.25	<0.0001	
W^{2*}	23.07	1	23.07	420.25	<0.0001	
P^{2*}	3.82	1	3.82	69.65	<0.0001	

Table 10: Continued.

Sources	Sum of squares	Degree of freedom	Mean square	F-value	*P* value	Significance
C^{2*}	8.26	1	8.26	150.49	<0.0001	
M^{2*}	13.69	1	13.69	249.5	<0.0001	
Residual	0.6038	11	0.0549			
Lack of fit	0.3354	6	0.0559	1.04	0.4926	Not significant
Pure error	0.2684	5	0.0537			
Cor total	69	32				
Std. deviation	0.234	R^2	0.9912			
Mean	3.64	Adjusted R^2	0.9753			
CV (%)	6.43	Predicted R^2	0.8684			
PRESS	9.08	Adeq. precision	23.5417			

error. An F-value this enormous could be the result of noise, according to the 49.26 percent probability. The expected R2 of 0.8684 is regarded fair because the difference between the expected R2 and the adjusted R2 is lesser than 0.2. The signal-to-noise ratio is determined by adequate precision. There should be a ratio of at least 4 is to 1. In this model, 23.5417 indicates a sufficient signal.

4. Conclusions

The following are significant findings gained from scientific research of incorporation of Mg and Cr filler in FSW uncoordinated connections of AA6063 and AA 5154:

(i) For highest TS, weld nugget hardness, and lowest corrosion rate, a multiobjective optimization of the RSM technique was applied and optimized the friction stir welding parameters.

(ii) An ideal input parameter for producing a sound joined aluminium alloy 6063 and aluminium alloy AA 5154 uncoordinated junction is a tool rotational speed of 1,000 rpm.

(iii) In terms of tensile strength, microhardness, and corrosion rate, tool rotating speed and powder mixing ratio are the two most important factors.

(iv) Weld nugget hardness of 93 HV and corrosion rate of 0.814 mm/y were achieved with the optimal parameter combination of R of 1000 rpm, W (120 mm/min), P (0.15 mm), C (2 mm), and M (95 percent Mg and 5 percent Cr) that was achieved.

(v) The joint strength of 147 MPa without filler was obtained by the above parameter combination.

(vi) The highest connection strength of 173 MPa was improved by mixing 95 percent magnesium and 5 percent chromium filler. This indicates that the use of filler in friction stir welding results in an 18 percent increase in joint strength.

(vii) Joint strength and weld hardness are originally increased by increasing the weight percentage of magnesium and reducing it by decreasing the chromium content in the alloy. A progressive drop in joint strengthening and weld hardness is observed following threshold value of 95 percent Mg and 5 percent Cr is crossed.

Data Availability

There is no data availability statement.

Conflicts of Interest

The authors declare that they have no conflicts of interest.

References

[1] J. Adamowski and M. Szkodo, "Friction stir welds (FSW) of aluminium alloy aw6063-T6," *Journal of Achievements in Materials and Manufacturing Engineering*, vol. 20, pp. 403–406, 2007.

[2] C. H. Cáceres, I. Svensson, and J. Taylor, "Strength-ductility behavior of Al-Si-Cu-Mg casting alloys in T6 temper," *International Journal of Cast Metals Research*, vol. 15, pp. 721–726, 2003.

[3] C. Jonckheere, B. De Meester, A. Denquin, and A. Simar, "Torque, temperature and hardening precipitation evolution in dissimilar friction stir welds between 6061-T6 and 2014-T6 aluminum alloys," *Journal of Materials Processing Technology*, vol. 213, no. 6, pp. 826–837, 2013.

[4] P. Cavaliere, A. De Santis, F. W. Panella, and A. Squillace, "Effect of welding parameters on mechanical and microstructural properties of dissimilar AA6082–AA2024 joints produced by friction stir welding," *Materials & Design*, vol. 30, no. 3, pp. 609–616, 2009.

[5] J. C. Feng, Y. C. Chen, and H. J. Liu, "Effects of post-weld heat treatment on microstructure and mechanical properties of friction stir welded joints of 2219-O aluminium alloy," *Materials Science and Technology*, vol. 22, no. 1, pp. 86–90, 2006.

[6] F. Mindivan, H. Kaya, M. Ozer, M. Uçar, and R. Samur, "Investigation of corrosion behavior of the AA5754 aluminum alloy joined using friction stir welding method," *Celal Bayar Üniversitesi Fen Bilimleri Dergisi*, vol. 11, no. 3, pp. 413–422, 2015.

[7] H. Fujii, L. Cui, M. Maeda, and K. Nogi, "Effect of tool shape on mechanical properties and microstructure of friction stir welded aluminum alloys," *Materials Science and Engineering: A*, vol. 419, no. 1-2, pp. 25–31, 2006.

[8] W. Gan, K. Okamoto, S. Hirano, K. Chung, C. Kim, and R. H. Wagoner, "Properties of friction-stir welded aluminum alloys 6111 and AA 5154," *Journal of Engineering Materials and Technology*, vol. 130, no. 3, pp. 31007–31022, 2008.

[9] K. Kamal Babu, K. Panneerselvam, P. Sathiya et al., "Parameter optimization of friction stir welding of cryorolled AA2219 alloy using artificial neural network modeling with genetic algorithm," *International Journal of Advanced*

Manufacturing Technology, vol. 94, no. 9-12, pp. 3117–3129, 2018.

[10] U. G. Kang, J. C. Lee, S. W. Jeong, and W. J. Nam, "The improvement of strength and ductility in ultra-fine grained 5052 Al alloy by cryogenic- and warm-rolling," *Journal of Materials Science*, vol. 45, no. 17, pp. 4739–4744, 2010.

[11] J. Kangazian and M. Shamanian, "Microstructure and mechanical characterization of Incoloy 825 Ni-based alloy welded to 2507 super duplex stainless steel through dissimilar friction stir welding," *Transactions of Nonferrous Metals Society of China*, vol. 29, no. 8, pp. 1677–1688, 2019.

[12] S. Katoh, "Pulsed TIG welding of aluminium," *Welding International*, vol. 4, no. 12, pp. 944–953, 1990.

[13] G. Viswanathan, R. Praveen, L. Prabhu, and S. Prakash, "Evaluating the machining parameters for milling P20 HH mould steel using a specific end mill," *Materials Today Proceedings*, vol. 46, pp. 8248–8253, 2021.

[14] N. T. Kumbhar and K. Bhanumurthy, "Friction stir welding of Al 5052 with Al 6061 alloys," *Journal of Metallurgy*, vol. 2012, Article ID 303756, 7 pages, 2012.

[15] K.-J. Lee and E.-P. Kwon, "Microstructure of stir zone in dissimilar friction stir welds of AA6061-T6 and AZ31 alloy sheets," *Transactions of Nonferrous Metals Society of China*, vol. 24, no. 7, pp. 2374–2379, 2014.

[16] C. Y. Lee, W. B. Lee, J. W. Kim, D. H. Choi, Y. M. Yeon, and S. B. Jung, "Lap joint properties of FSWed dissimilar formed 5052 Al and 6061 Al alloys with different thickness," *Journal of Materials Science*, vol. 43, no. 9, pp. 3296–3304, 2008.

[17] W. B. Lee, Y. M. Yeon, and S. B. Jung, "The mechanical properties related to the dominant microstructure in the weld zone of dissimilar formed Al alloy joints by friction stir welding," *Journal of Materials Science*, vol. 38, pp. 4183–4191, 2003.

[18] C. Leitao, R. M. Leal, D. M. Rodrigues, A. Loureiro, and P. Vilaca, "Mechanical behaviour of similar and dissimilar AA5182-H111 and aa6016-T4 thin friction stir welds," *Materials & Design*, vol. 30, no. 1, pp. 101–108, 2009.

[19] M. M. El-Rayes and E. A. El-Danaf, "The influence of multi-pass friction stir processing on the microstructural and mechanical properties of Aluminum Alloy 6082," *Journal of Materials Processing Technology*, vol. 212, no. 5, pp. 1157–1168, 2012.

[20] M. Peel, A. Steuwer, M. Preuss, and P. J. Withers, "Microstructure, mechanical properties and residual stresses as a function of welding speed in aluminium AA5083 friction stir welds," *Acta Materialia*, vol. 51, no. 16, pp. 4791–4801, 2003.

[21] D. A. Baiseitov, S. Tursynbek, L. Sassykova et al., "Research of the combustion of gas-generating compositions with additives of carbon powders," *Materials Today Proceedings*, vol. 33, pp. 1216–1220, 2020.